EFFECTS OF VISCOELASTICITY ON THE DEPLOYMENT OF BISTABLE TAPE SPRINGS

A. Brinkmeyer[1,2*], S. Pellegrino[2], P. M. Weaver[1], M. Santer[3]
[1] ACCIS, Department of Aerospace Engineering, University of Bristol, Bristol, United Kingdom
[2] GALCIT, California Institute of Technology, Pasadena, CA, USA
[3] Department of Aeronautics, Imperial College London, London, United Kingdom
* Corresponding author (alex.brinkmeyer@bristol.ac.uk)

Keywords: *composites, bistability, viscoelasticity, deployable, STEM*

Abstract

The effects of stowage on the deployment of composite bistable tape springs are studied. A viscoelastic analytical model is used to predict the relaxation and stability of the structure in its coiled state. The time-dependent stability analysis reveals that the structure remains bistable throughout the relaxation process. A dynamic model is then applied to predict the deployment of the structure once it is released. Experimental deployment results match the deployment predictions within 3% for the case where no stowage is applied. It is shown that stowage causes an increase in the deployment time; in this case, experimental deployment times overshoot those predicted by the model. Secondary effects are observed at high stowage temperatures, which are not predicted by the analytical model. These effects include an abrupt change in the deployment dynamics and a large increase in the deployment time (deployment latency). At higher temperatures still, i.e. for stowage at 100°C, the structure fails to deploy and becomes stable at all extended lengths.

1 Introduction

A novel investigation into the deployment kinematics of fiber-reinforced bistable tape springs is conducted taking into account the effects of viscoelasticity. These structures are based on the concept of the Storable Tubular Extendable Member (STEM). STEMs have gained popularity in space applications and were used, for example, to deploy the solar arrays of the Hubble telescope [1]. Tape springs, in constrast with STEMs, are designed to be bistable; this concept, commercialized by RolaTube in 1997 [2], has been since then used in various civil and military applications.

In this research, the tape springs are manufactured using an ultra-thin carbon fiber composite material and an asymmetric layup. The resulting structure is stable in its coiled state and can be stowed in a small volume. When deployed, the structure rapidly extends into an open-section boom (Fig. 1). Viscoelastic effects have been reported in similar structures [1, 3], but not yet studied in depth for bistable tape springs; this is the main aim of this paper.

First, we study how the relaxation of the material affects the stability of the coiled structure. Secondly, a simple dynamic model is applied to predict the change of deployment speed with the different stowage conditions (duration and temperature) and to use experimental tests to validate the model predictions.

The results from this investigation are thought to be useful in quantifying the effects of viscoelasticity in long-term stowage and deployment of tape springs and providing insight into the design of these structures.

2 Geometry and material definitions

2.1 Geometry

This work considers the following stowage and deployment process. The structure—initially manufactured in its extended shape—is coiled fully and stowed at a given temperature. At the start of the deployment, one end of the coil is snapped out and restrained. The other end of the structure is then allowed to deploy. The position of the center of the coil is then measured with time.

The structure in its coiled state is associated with a radius r, while the uncoiled state has a radius R. The uncoiled structure subtends an angle β, and has a total length L (Fig. 2). We assume throughout that the structure exists either in its coiled or uncoiled state (the transition zone 'T' is neglected).

2.2 Material properties

The material used is ThinPly T800H, an ultra-thin unidirectional carbon fiber prepreg with ply thickness 31 μm. The material elastic properties at room temperature have been determined experimentally and are given in Table 1.

In this research we use the anti-symmetric layup $[45/-45/0/45/-45]$. The 0° direction is oriented along the length of the tape spring. An anti-symmetric layup is used to reduce the bend-twist effects otherwise present in a symmetric layup because of a full **D** bending stiffness matrix.

The analytical model consists of three parts, which are described in more detail in the following sections:

1. *Stowage model*: Transforms the material relaxation data obtained at ply level to the overall laminate relaxation using Classical Laminate Analysis.
2. *Stability model*: Uses a stability criterion to determine whether the structure is bistable and how the degree of stability evolves with relaxation.
3. *Deployment model*: Uses the material state at the end of the relaxation step to predict the dynamic deployment of the tape spring.

3 Stowage model

3.1 Ply level relaxation

Relaxation tests on $[90]_6$ specimens have been performed to determine the viscoelastic behavior in transverse tension $E_{22}(t)$. It is assumed that since the carbon fibers are not viscoelastic, no relaxation occurs in the longitudinal direction, so $E_{11}(t) = E_0$.

An Instron machine equipped with a thermal chamber was used for the tests. The specimen and the Instron grips were first allowed to warm to the set temperature for around 2 hrs; this was to allow the entire rig to achieve thermal equilibrium prior to the relaxation test. The rig was then adjusted to remove any slack induced by temperature effects, and the specimen was allowed to rest for another 30 min. Transient thermal expansion of the rig was found to have a large influence on the relaxation results, as thermal expansion strains were of the same order as the mechanical strains. Hence, achieving thermal equilibrium prior to the test was crucially important for accurate results.

The relaxation test consisted of applying a quasi-instantaneous strain of 0.1% to the specimen and holding this value for 3 hrs. The load and strain were recorded through a 3D Digital Image Correlation (DIC) system (Fig. 3). It was found that the calculation of the instantaneous modulus $E_{22,0}$ from the relaxation test was inaccurate because of the small strains involved. Hence, a tensile test was subsequently used to determine $E_{22,0}$ at each temperature to complete the characterization of the material.

A Prony series is assumed to represent the relaxation behavior of the material, where $e_{\mathrm{R}i}$ are the tensile relaxation coefficients associated with the transverse modulus $E_{22}(t)$, τ_i are the retardation times, and N are the number of terms.

$$\frac{E(t)}{E_0} = 1 - \sum_{i}^{N} e_{\mathrm{R}i}\left(1 - e^{t/\tau_i}\right). \qquad (1)$$

A similar expression can be defined for the shear modulus, where $g_{\mathrm{R}i}$ are the shear relaxation coefficients associated with the shear modulus $G_{12}(t)$. It is assumed that the Poisson's ratio is time-independent, hence it is possible to set $e_{Ri} = g_{Ri}$ without loss of validity.

A four-term Prony series is fitted to the experimental data curves fitting using a MATLAB nonlinear optimization algorithm. An example of the fitting of the relaxation curve for stowage at 60°C is given in Fig. 4; the Prony series is given in Table 2.

3.2 Laminate-level relaxation

A Classical Laminate Analysis (CLA) method is used to transform the lamina stiffnesses $E_{22}(t)$ and $G_{12}(t)$ to laminate stiffnesses $Q^*_{ij}(t)$, and finally to the laminate bending stiffnesses $D_{ij}(t)$.

The evolution of the laminate bending stiffness components with relaxation time is shown in Fig. 5. D_{11}, D_{22}, and D_{66} decrease with time, whilst D_{12} increases. The D_{16} and D_{26} components are not shown in the figure.

The increase in the D_{12} term may seem counter-intuitive, but an analysis using lamination parameters shows that D_{12} increases if and only if

$$\frac{E_{22}}{G_{12}} < \frac{4(1-\nu_{12}\nu_{21})}{1+2\nu_{12}}$$

This expression is satisfied in this case, as $E_{22}/G_{12} = 0.86$ and the right hand side is equal to 2.06.

A complete proof is given in Brinkmeyer [4].

3.3 Time temperature superposition

The time-temperature superposition (TTS) principle for linear viscoelastic materials is used to generalize the analytical model to other temperatures and stowage times [5]. The TTS principle states that increasing the temperature of test of the material is equivalent to a shift a_T in the relaxation time.

The time shift is given by the following relationship

$$\log(a_T) = -\frac{C_1(T-T_r)}{C_2+(T-T_r)} \qquad (2)$$

Using experimental characterization at 40°C, 60°C, 80°C, and 100°C, the constants in Equ. 2 have been determined to be $C_1 = -1.35$ and $C_2 = 42.9$, for a reference temperature of $T_r = 60$°C.

With this model, the relaxation of the material can be generalized to any temperature T by substituting the time t in Equ. 1 by the reduced time t'. At a given temperature T, the reduced time t' is given by

$$t' = \frac{t}{a_T(T)} \qquad (3)$$

4 Stability

4.1 Stability criterion

A criterion of bistability for curved tubes, developed by Guest and Pellegrino [6], is used to determine the stability of the coiled structure. This criterion S is given by

$$S = 4\widehat{D}^*_{66} + 2\widehat{D}^*_{12} - 2\frac{\widehat{D}^*_{22}}{\widehat{D}^*_{12}}, \qquad (4)$$

where $\widehat{\mathbf{D}}^*$ is the non-dimensional reduced bending stiffness, given by $\widehat{\mathbf{D}}^* = \mathbf{D}^*/D^*_{11}$ and $\mathbf{D}^* = \mathbf{D} - \mathbf{BA^{-1}B}$.

Guest showed that if $S > 0$ then the tube is bistable, and if $S \leq 0$ the structure is monostable. It was also found that isotropic structures do not yield bistable structures, unless they are pre-stressed (the familiar carpenter's tape, for instance, is an example of a pre-stressed bistable tape spring). In fact, it can be shown that for isotropic layups, $S \leq -2$ for all ν, hence demonstrating that preformed isotropic structures are not suited for this application. Using a composite layup, on the other hand, seems appropriate, as the stiffness can be tailored according to the application and S can be chosen to be positive.

We now extend the stability criterion to general viscoelastic composite structures, by introducing a variation of the non-dimensional constants with time; hence, the stability criterion becomes

$$S(t) = 4\widehat{D}^*_{66}(t) + 2\widehat{D}^*_{12}(t) - 2\frac{\widehat{D}^*_{22}(t)}{\widehat{D}^*_{12}(t)} \qquad (5)$$

The $[45/-45/0/45/-45]$ layup was chosen as it yielded a suitably bistable structure, with an initially positive stability value of $S(0) = 0.95$. We now investigate how the stability of the structure changes with relaxation.

4.2 Stability results

We first study the change with time of the three non-dimensional parameters composing S, i.e. $\widehat{D}_{12}^*$, $\widehat{D}_{22}^*$, $\widehat{D}_{66}^*$. These are plotted in Fig. 6 for stowage of the structure at 60°C for 3 hrs. The plot shows that, contrary to the stiffnesses in Fig. 5, both $\widehat{D}_{12}^*$ and $\widehat{D}_{66}^*$ increase with relaxation time, while $\widehat{D}_{22}^*$ remains approximately constant. It is noted that this graph is representative of a general stowage case.

Returning to the definition of the stability criterion (Equ. 5), it becomes clear that the $\widehat{D}_{12}^*$ and $\widehat{D}_{66}^*$ terms increase and the $\widehat{D}_{22}^*/\,\widehat{D}_{12}^*$ term decreases. Hence, S increases with time. The plot of the stability criterion with relaxation time confirms the rise of the stability criterion with time (Fig. 7), with S increasing from $S = 1.2$ for $t = 1\,s$ to $S = 2.05$ for $t = 3$ hrs. In other words, if the structure is initially bistable, the structure *remains bistable* at all times during relaxation. In other words, the tape spring will not self-deploy once it is stored in its coiled state.

5. Deployment model

In the deployment experiment the spring is initially coiled and allowed to relax. Then, the tip of the coil is fixed at one end and the spring is allowed to extend at the other (Fig. 2). Here, we use an analytical deployment model, based on work by Rimrott [7] and Iqbal [1], to predict the deployment of the spring. The model, originally derived for isotropic STEMs, has here been generalized to orthotropic viscoelastic laminates. This model assumes that the structure immediately transitions from a coiled shape to an extended shape. In reality, however, the transition occurs smoothly within a transition zone (indicated by 'T' in Fig. 2).

The bending strain energy in a composite shell, deformed such that the curvature changes are κ_x and κ_y is shown to be [1]

$$U_b = \frac{1}{2}[\kappa_x \quad \kappa_y \quad \kappa_{xy}]\ \boldsymbol{D}\ \begin{bmatrix}\kappa_x\\ \kappa_y\\ \kappa_{xy}\end{bmatrix} A \qquad (6)$$

where A is the cross sectional area per unit thickness given by $A = \beta R x$.

Here we assume that $\kappa_{xy} = 0$ and $D_{16} = D_{26} = 0$ so Equ. 6 reduces to

$$U_b = \frac{1}{2}\left(D_{11}\kappa_x^2 + 2D_{12}\kappa_x\kappa_y + D_{22}\kappa_y^2\right)A \qquad (7)$$

Setting $\kappa_x = 1/r$ and $\kappa_y = -1/R$ then the strain energy becomes

$$U_b = \frac{D_{11}\beta x}{2R}\left[1 + \left(\frac{R}{r}\right)^2 \frac{D_{22}}{D_{11}} - \frac{2R}{r}\frac{D_{12}}{D_{11}}\right] \qquad (8)$$

The ejection force driving the tube forward is given by the rate of change of the strain energy with respect to the extension [6], hence

$$F_e = \frac{\partial U_b}{\partial x} \qquad (9)$$

We apply a correction for non-symmetric laminates by using the reduced bending stiffness $\mathbf{D}^*$. Using the non-dimensional notation $\widehat{\mathbf{D}}^* = \mathbf{D}^*/D_{11}^*$ and letting the bending stiffness constants vary with time, the ejection force is finally given by

$$F_e(t) = \frac{D_{11}^*(t)\beta}{2R}\left[1 + \left(\frac{R}{r}\right)^2 \widehat{D}_{22}^*(t) - \frac{2R}{r}\widehat{D}_{12}^*(t)\right]. \qquad (10)$$

The ejection force only exists when the tape spring is being deployed; however, we can simulate the evolution of the stored strain energy with time and predict how the ejection force would decrease with stowage time. This is shown in Fig. 8 for stowage at 60°C for 3 hrs.

For deployment in air, a simple aerodynamic drag model is implemented to adjust the net ejection force. The drag of the structure is given by

$$F_{\text{aero}}(t) = 0.5\rho V^2(t) C_D A. \qquad (11)$$

The frontal area A is based on the coiled shape of the spring and is given by $A = 2\beta R r$. The drag coefficient C_D is based on the average Reynolds number Re. For this application it can be shown that $Re \approx 1000$, so $C_D \approx 1.17$.

We assume that the ejection force does not change during deployment, as the deployment occurs over a much shorter time scale than relaxation; hence we take the ejection force at the end of relaxation as the input for the deployment model, $F_e = F_e(t = t_{rel})$, where t_{rel} is the total relaxation time.

As the drag acts in opposite sense to the deployment direction, the net ejection force is therefore given by

$$F(t) = F_e - F_{aero}(t). \quad (12)$$

Finally, using an energy method initially developed by Rimrott [7], it can be shown that the ejection velocity is given by

$$v(t) = \sqrt{\frac{F(t)(1-\mu)x}{m(L-x)}} \quad (13)$$

where μ is a friction coefficient, L is the total length of the tube, and m the mass per unit length. The empirical value $\mu \approx 0.6$ was found to be appropriate [6]. A simple iterative method is then used to integrate the velocity to obtain the position of the tape spring with time.

Plotting the deployment curve with and without the aero correction shows that drag has little effect on the dynamic behavior (Fig. 9). A slight deviation from the two curves is visible near the end of deployment (where the velocity is highest), with an increase of around 2% in deployment time. It is expected, however, that for much longer (> 10 m) and larger structures, aerodynamic effects will play a larger role.

6 Deployment experiments

6.1 Manufacture

The originally flat laminate is first molded onto a male cylindrical mandrel. Shrink tubing is then used to secure the laminate onto the mold. Breather fabric and a vacuum bag are then fitted around the mandrel and sealed. The assembly is then cured at 120°C for 3 hrs using an aerospace-grade autoclave.

Surface wrinkles on the cured tape spring are a major source of experimental error as the wrinkles considerably increase the local laminate thickness, hence bending stiffness. The use of a shrink tube serves to considerably reduce the risk of surface wrinkles, which otherwise form as the exterior bag crumples under the applied vacuum.

The manual layup of the prepreg is complicated by the material is very thin and difficult to handle. We suggest that future work should use an appropriate automated tape laying apparatus, as indicated by the manufacturer, to improve the quality of the finished product and to increase the ease of manufacture.

Although an anti-symmetric layup has been chosen to reduce bend-twist effects, the resulting structure still presents a significant amount of twist (around 140°/m after demolding). This is clearly apparent in Fig. 10. This is due to significant residual thermal strains appearing in the laminate on cool-down as a result of layup antisymmetry. The overall small thickness of the laminate accentuates this effect, which may be why this result has not been reported in previous research [1]. In future work, a symmetric layup should be considered as an alternative to reduce the net twist in the finished structure.

6.2 Deployment set-up

In the experiments, the specimen was coiled then stored in the Instron thermal chamber for 3 hrs at the set temperature. A thermocouple is used to ensure that the structure has reached the correct temperature. Two stowage cases are investigated, 60°C and 100°C.

At the end of the stowage period, the structure is removed from the chamber and deployed at room temperature on a flat, horizontal surface. (This is because it is impractical to perform the deployment within the thermal chamber.) A camcorder is used to record the deployment of the tape spring at a frame rate of 29 fps. A video editor is then used to determine the position of the center of the coil for each time frame.

Prior work has shown that there is no significant difference in deploying the structure at room temperature rather than at the temperature at which it has been stowed [3]. This is mainly because the deployment occurs over a much shorter time scale

than the relaxation. Hence, it is possible to neglect viscoelastic effects during the deployment and assume that deploying the structure at room temperature has little effect on the deployment behavior.

6.3 Comparison with the analytical model, without stowage

The deployment photographs (Fig. 11) show a rapid and generally smooth unrolling of the structure. However, near the end of the deployment, the assumption of uniform uncoiling breaks down. In this region, the tape spring starts to unravel laterally (Fig. 11c), followed by a dynamic latching of the tip. Therefore, it is convenient to neglect the final uncoiling of the structure and compare the time it takes to achieve 90% deployment.

Fig. 12 compares the analytical and experimental deployment curves for the case without stowage. The curves confirm that the overall deployment is smooth and uniform, and that the rate of deployment increases with time. Visibly, experimental and analytical results match closely, with a slight overestimation of the deployment time by the analytical model. Here, the analytical model predicts a 90% deployment time of 0.41 s, compared with 0.40 s in the experiment, i.e. a 2.5% difference.

6.4 Comparison with analytical model, with stowage at 60°C

We now consider the case where the tape spring is stowed at 60°C for 3 hrs prior to deployment. Fig. 13 compares the deployment curves for both cases with and without stowage. Where stowage is applied, the curves exhibit a clear decrease in the deployment rate and hence an increase in the deployment time. The analytical model supports this observation. It has previously been shown that stowage causes a decrease in the ejection force. Returning to Equ. 13, a decrease in the ejection force would cause the deployment velocity to drop, which is the effect observed here.

The analytical results for the stowed configuration do not match the experimental results as well. Here, the analytical model visibly underestimates the deployment time, with the analytical model predicting a 90% deployment in 0.52 s, while the experiment shows a deployment in 0.57 s (i.e. an underestimation of 9%).

Overall, it is seen that the error between the experimental and predicted curves increases with stowage, i.e. viscoelastic relaxation. This suggests that the actual ejection force is in fact lower than predicted; this could be due to errors in material characterization or could also suggest that a refinement of the dynamic model is needed. In the current model we assume a single coefficient of friction μ, similar to Coulomb friction, to represent the loss of ejection force. (Friction can indeed occur during the deployment process, e.g. as a result of coils sliding across each other.) Nevertheless, further experimental work would be needed to better understand the role of frictional forces—or other dissipative mechanisms—in the deployment of the tape spring.

6.5 Deployment latency

The previous results have shown that the stowage of the tape spring leads to an increase in the deployment time. In most of the cases observed until now, the deployment remains continuous and consists of a rapid dynamic deployment of the spring once the constraint has been released. This is what we name *Type I* deployment.

It has been observed in certain cases, however, that the deployment of the tape spring is not continuous and consists of two distinct behaviors. The first is a latent region where no or little movement is observed, even though the tape spring is no longer restrained. The second is the normal dynamic deployment observed previously. We call this *Type II* deployment.

Fig. 14 shows the deployment curve for a tape spring stowed at 60°C for 3 hrs for this type of deployment. The latent region lasts in this case for around 0.45 s, before the spring deploys dynamically in 0.55 s. Total deployment lasts around 1.0 s, which is nearly twice as higher as the dynamic deployment shown in Fig. 14. We note that the dynamic deployment is the same in both Type I and II deployments. Also, the latent region is subject to

typically large variations, making it difficult to predict the total deployment time.

The fact that this latent behavior appears only in tubes that have been stowed at high temperature suggests that this is an effect linked to viscoelastic relaxation effects. Second, it seems that the analytical model is inadequate to capture these latency effects. These secondary effects may arise from local effects in the transition zone, which are not predicted by the model. A numerical model would be needed to understand these effects better.

It is important to recall at this point previous research on the phenomenon of pseudo-bistability—a self-actuation phenomenon due to viscoelastic relaxation effects [8]. It was previously noted that pseudo-bistability is a result of a structure transitioning between a monostable and a bistable system under viscoelastic relaxation. It was also shown that the deployment of a pseudo-bistable structure was characterized by two different time scales—a slow recovery, followed by a sudden dynamic recovery. It can be suggested that the latent behavior of the tape springs can be described as a local pseudo-bistable effect, which causes the appearance of this latent deployment region.

6.6 Deployment failure

The stowage of the tape spring at 100°C for 3 hrs represents a peculiar case. For this stowage configuration, the tape spring fails to deploy altogether. Fig. 15 shows an overlay of photographs of the deployment of the spring after stowage at 100°C for 3 hrs. The spring is found to be stable at any extended position, including the fully deployed case. This goes to show that the net ejection force of the structure has dropped to zero, and that the structure does not have sufficient stored strain energy for an autonomous deployment. In other words, the structure has transitioned from being bistable to neutrally stable.

The fact that the structure seems to have gained additional states of stability is coherent with the result from Section 4—i.e. that the stability criterion of the structure increases with time. Nevertheless, the analytical analysis that led to this result is not sufficient to explain what appears to be a local stability effect.

This could be potentially catastrophic if the sole function of the tape spring were to be autonomous deployment.

6.7 Aging & hysteresis

Due to experimental constraints, only two tape spring prototypes were used in the deployment test, with one being preferred over the other because of superior surface finish (no wrinkles). Each deployment test was performed several times on the same specimen on different days to determine the repeatability of the tests. Between the tests, the specimen was allowed to recover for at least one day.

Results reveal that the deployment time increases with the age of the specimen, and seems to settle at an asymptotic value. Fig. 16 shows this effect for the case without stowage on four successive (but not consecutive) days.

It is suggested that the processing of the specimen at higher temperature intervals may induce a post-cure or aging effect, which would increase the transition glass temperature upwards from 120°C. This would result, however, in a reduction in material relaxation at a given temperature in the glassy region, i.e. a decrease of the deployment time. This is not consistent with the results obtained.

A better explanation could be that the structure exhibits a strong hysteresis effect. Storing the tube at room temperature in the extended position for one or two days may be insufficient to recover the initial stiffness completely.

Finally, it is suggested that moisture may also have an effect on the deployment behavior. It has been observed that the residual twist in the laminate reduces with exposure time to ambient air, which suggests moisture ingress [9]. The resulting change in the geometry may then influence the recovery behavior to a slight extent.

A more detailed study on these effects will be needed to ascertain the exact underlying mechanism.

7. Conclusions & future work

In conclusion, this work has shown that relaxation effects due to stowage of the tape spring in a coiled state causes significant changes in the deployment behavior of the structure.

Stowage the structure at higher temperature or for longer periods of time *increases* the dynamic deployment time of the structure by decreasing the stored strained energy available for deployment. This may be beneficial in reducing dynamic latching effects associated with a rapid deployment, and hence reduce the risk of fracture of the material.

We have shown that the stability of the structure always increases with relaxation, which means that an initially bistable structure will not self-deploy once in its coiled state.

In cases where the relaxation of the structure is significant, secondary deployment effects appear. For instance, stowage at 60°C for 3 hrs causes a significant delay prior to the dynamic deployment of the structure—i.e. *deployment latency*. This effect is not yet well understood and is thought to be due to local stability effects. The time associated with deployment latency is difficult to predict but can be shown to increase with relaxation.

For stowage at 100°C for 3 hrs, the tape spring fails to deploy altogether and remains stable at any deployed position. The deployment latency time has risen to infinity, and the structure has gained neutral stability. Although these observations are consistent with an increase of the stability criterion, the latter is not sufficient to capture what seems to be a local stability effect.

The possibility of deployment failure for high-stowage configurations is an important result of this research, which should be taken into account when designing bistable deployable structures. It is noted that, should deployment failure occur, an actuator would be needed to achieve the full deployment of the structure. On the other hand, the neutral stability of the tape spring gained through relaxation can be used as an advantage to reduce the actuator power requirements.

Future work will focus on better understanding the effects of viscoelastic relaxation on the deployment of the structure using a numerical finite element model.

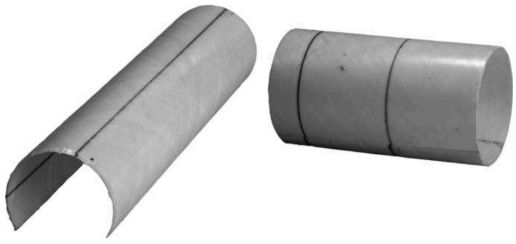

Fig. 1. Bistable tape springs in coiled and uncoiled configurations [1].

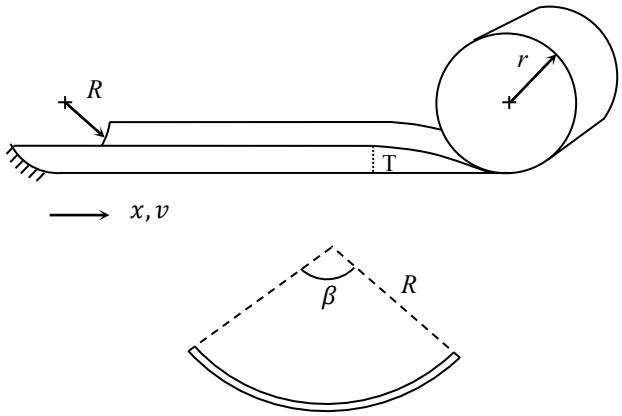

Fig. 2. Geometry of bistable tape spring. R and r are respectively the initial and deployed radii, β is the subtended angle, and the total deployed length is L. Here R = 16.6 mm, r = 20.8 mm, β = 131.8° and L = 1253 mm.

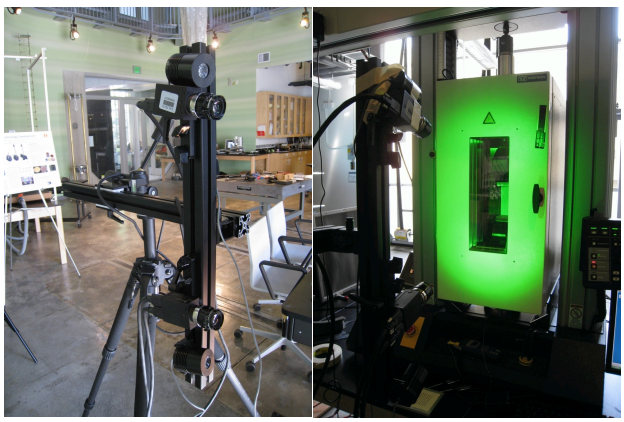

Fig. 3. Relaxation test apparatus. Left, stereoscopic DIC camera system with green lights. Right, thermal chamber mounted in Instron tensile testing machine.

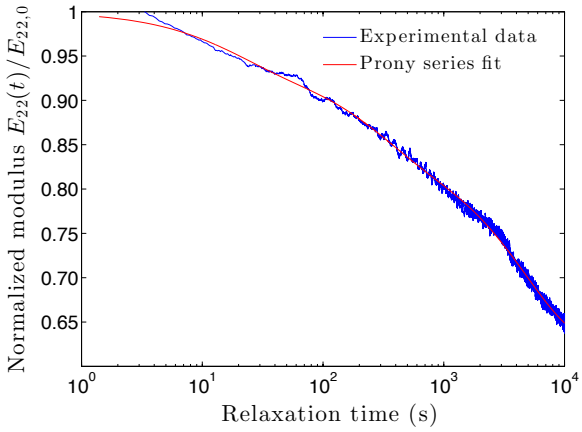

Fig. 4. Plot of the normalized transverse modulus $E_{22}(t)/E_{22,0}$with Prony series fit for relaxation at 60°C for 3 hrs (approximately 10^4 s).

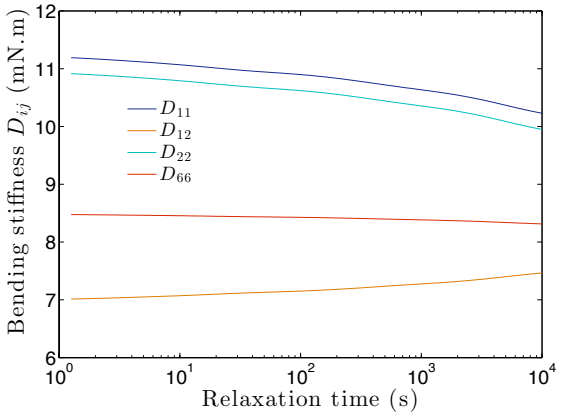

Fig. 5. Plot of the D_{ij} bending stiffness components with relaxation time for stowage at 60°C for 3 hrs.

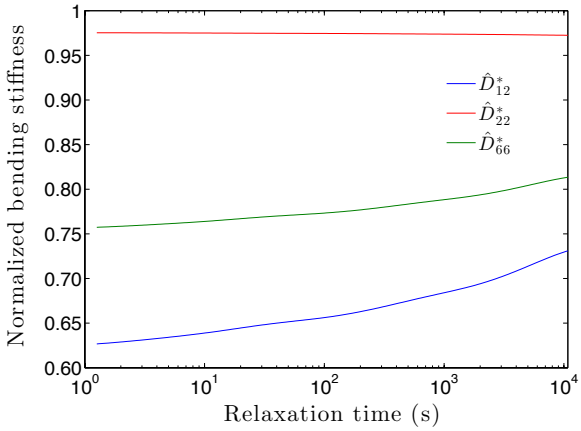

Fig. 6. Plot of the normalized bending stiffnesses with relaxation time. As the tape spring relaxes, $\widehat{D}^*_{12}$ and $\widehat{D}^*_{66}$ increase, while $\widehat{D}^*_{22}$ remains constant.

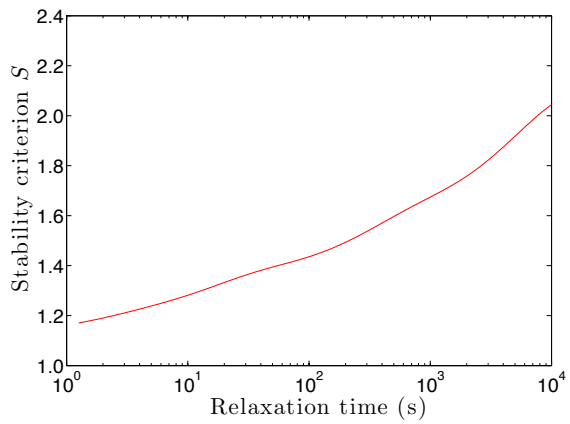

Fig. 7. Evolution of the stability criterion with stowage time. The criterion is positive for all *t*, hence the structure remains bistable during relaxation.

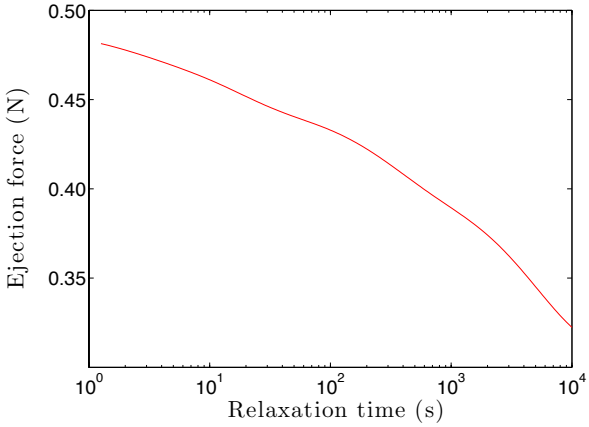

Fig. 8. Plot of the ejection force with relaxation time for stowage at 60°C for 3 hrs.

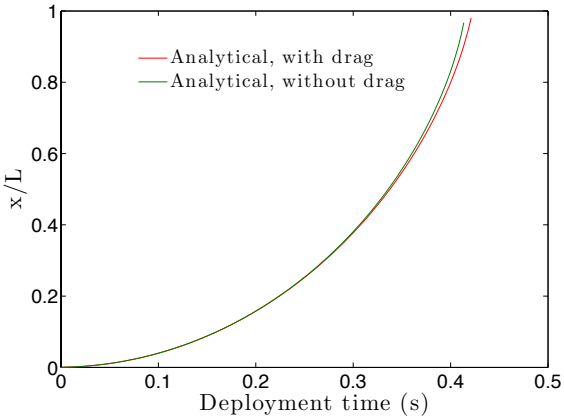

Fig. 9. Deployment curves with and without the drag correction, for the case without stowage.

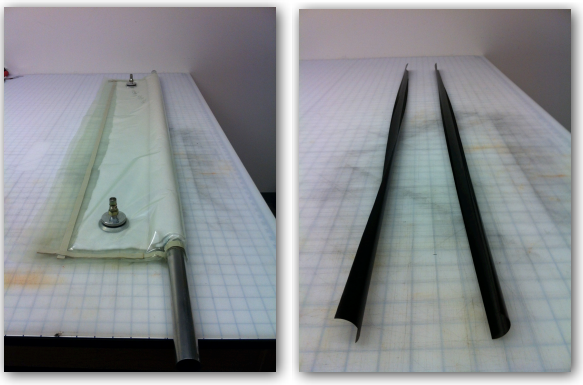

Fig. 10. Manufacture of the tape spring. Left: completed vacuum bag with ports visible. Right: finished product showing the twist in the structure.

Fig. 11. Snapshots of the deployment of the tape spring. (a) t = 0.10 s, (b) t = 0.28 s, (c) t = 0.40 s, (d) t = 0.44 s.

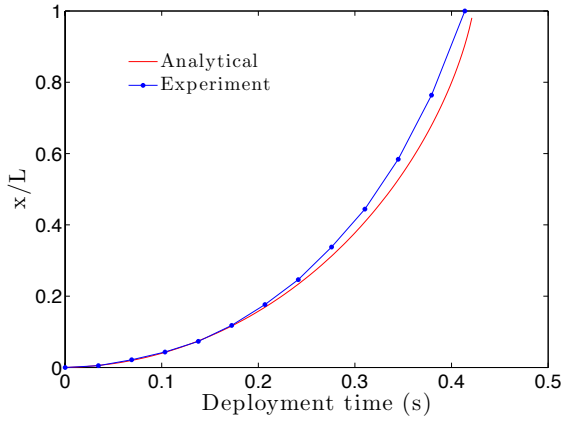

Fig. 12. Deployment comparison for analytical and experimental results for $\mu = 0.6$.

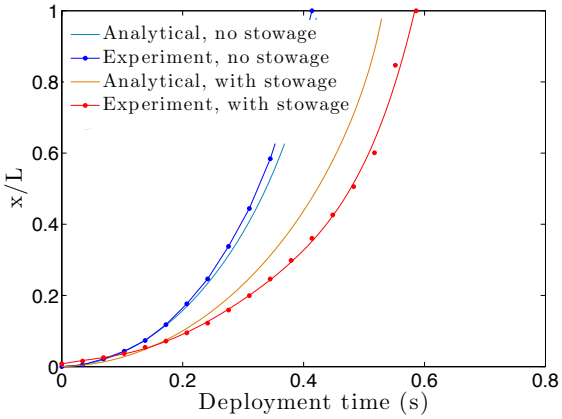

Fig. 13. Comparison of the deployment profile for stowage at 60°C for 3 hrs and without stowage (Type I deployment).

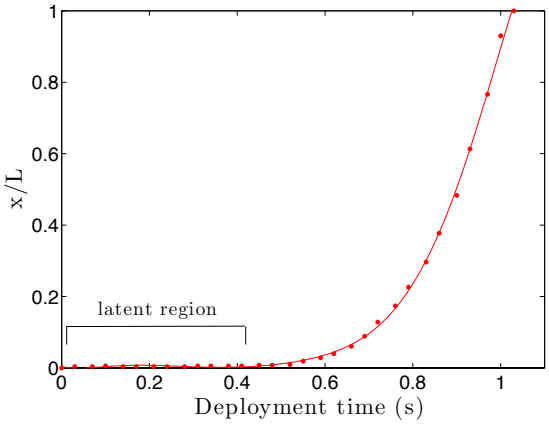

Fig. 14. Deployment profile for tape spring stowed at 60°C for 3 hrs (Type II deployment with latency). The latent region lasts around 0.45 s.

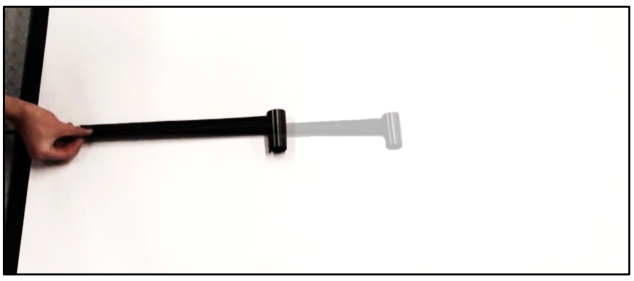

Fig. 15. Overlay of photographs of the deployment of the tape spring at room temperature after stowage at 100°C for 3 hrs. The structure is stable for any deployed length.

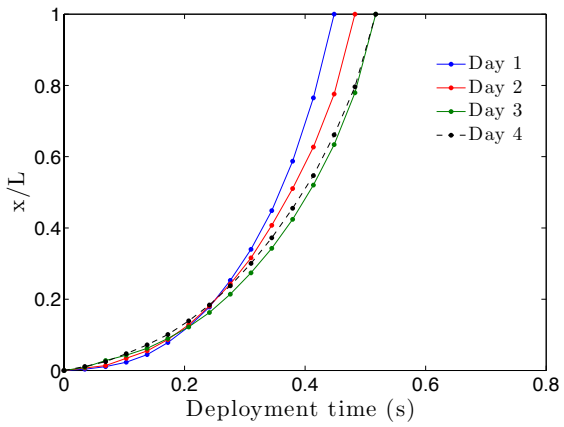

Fig. 16. Deployment curves for the case without stowage on different testing days. Deployment time increases with the age of the specimen (the days are not consecutive.)

Table 1. T800H ThinPly elastic properties at room temperature. The subscript '0' denotes instantaneous conditions.

E_{11} (GPa)	$E_{22,0}$ (GPa)	$G_{12,0}$ (GPa)	ν_{12} (-)
128	6.5	7.6	0.35

Table 2. Prony series of transverse modulus E_{22} at 60°C.

N	e_{Ri}	τ_i
1	0.013	2.64
2	0.062	16.3
3	0.094	266
4	0.219	4790

References

[1] K. Iqbal "*Mechanics of Laminated Bistable Tubular Structures"*. PhD Thesis, 2001.

[2] Rolatube. Our Business. http://www.rolatube.com/our-business. Accessed April 20, 2013.

[3] Kwok, K. and Pellegrino, S. (2011). Viscoelastic effects in tape springs. *52nd AIAA/ASME/ASCE/AHS/ASC Structures, Structural Dynamics and Materials Conference*, 4-7 April 2011, Denver, CO, AIAA 2011-2022.

[4] Brinkmeyer, A. *Time Dependent Bistable Morphing Composites*. PhD Thesis, 2013.

[5] Ferry, John D. Viscoelastic properties of polymers. Vol. 641. New York: Wiley, 1980.

[6] Guest, S. D. and Pellegrino, S. Analytical models for bistable cylindrical shells". *Proceedings of the Royal Society*, Vol. 462, pp. 839-854, 2006.

[7] F. P. J. Rimrott. STEM Self-extension velocities. *Canadian Aeronautics and Space Journal*, Vol. 13 (1), pp. 1-7, 1967.

[8] Brinkmeyer, A., et al. Pseudo-bistable self-actuated domes for morphing applications. *International Journal of Solids and Structures*, Vol. 49, pp 1077 – 1087, 2012.

[9] Etches, J., et al. Environmental effects on thermally induced multistability in unsymmetric composite laminates. *Composites Part A: Applied Science and Manufacturing*, Vol. 40 (8), pp. 1240-1247, 2009.